LUND UNIVERSITY

Instrument Development - Cloud Condensation Nuclei Counter

Elin Svensson

Lund University, Department of Physics

Academic advisors: Birgitta Svenningsson, Cerina Wittbom

Submitted: 2013-06-05

Abstract

A cloud condensation nuclei counter (CCNC) is used to study the ability of aerosol particles to serve as cloud condensation nuclei (CCN) depending on their size, chemical composition and the ambient water super saturation. In this study, the new operation mode *Scanning Flow CCN Analysis* (SFCA) was evaluated for the Continuous-Flow Streamwise Thermal-Graident Cloud Condensation Nuclei Counter from Droplet Measurement Technologies (CCNC DMT-100). By continuously changing the flow rate through the instrument, while keeping the streamwise temperature gradient and pressure constant, the SFCA enables measurements of entire super saturation spectra with high temporal resolution.

The SFCA was evaluated for three magnitudes of the streamwise thermal gradient (4, 10 and 18 K) using three types of calibration particles (sodium chloride, ammonium sulfate and sucrose). By examining the flow rates at which the particles activated into cloud droplets, the critical flow rates could be related to the critical super saturations found from Köhler theory. In this way, calibrations between the flow rates and super saturations of the CCNC were obtained. Nine calibration curves were obtained in total, one for each substance and streamwise temperature gradient. To verify the validity of the curves, 95% confidence intervals were calculated. The calibration curves were then compared with each other to evaluate the reability of the operation mode. The SFCA was found to be reliable for streamwise temperature gradients of 4 and 10 K, but somewhat less reliable for a temperature gradient of 18 K. The calibration curves were also found to be the least reliable at the ends.

Contents

1 Introduction

Clouds exert a great effect on climate, regulating the temperature on earth by reflecting incoming solar radiation and preventing terrestrial radiation from escaping the atmosphere, as well as determining earth's hydrological cycle. To be able to understand and predict the climate, it is therefore essential to gain knowledge about cloud physics. Cloud formation is one of the processes that has become increasingly important to understand due to the recent increase in anthropogenic emissions. Many of the emitted particles serve as *cloud condensation nuclei* (CCN) and are thereby cloud droplet precursors.

Cloud droplets form by condensation of water vapor onto atmospheric *aerosol particles*. An aerosol is defined as an airborne suspension of small solid and/or liquid particles [1]. In this study however, the word aerosol will refer to the particulate component only. A droplet is first considered to be a cloud droplet when its equilibrium vapor pressure decreases with an increasing diameter [2]. The droplet is then said to be activated and the aerosol has served as a CCN. It is of great interest to examine the ability of aerosols to serve as CCN depending on their size, chemical composition and the ambient water super saturation.

The ability of aerosols to serve as CCN can be examined by a CCN Counter (CCNC). This study aims at evaluating the new operation mode *Scanning Flow CCN Analysis* (SFCA) of the Continuous-Flow Streamwise Thermal-Graident Cloud Condensation Nuclei Counter from Droplet Measurement Technologies (CCNC DMT-100). By continuously changing the flow rate through the instrument, the SFCA enables measurements of entire super saturation spectra with high temporal resolution. In this study, calibrations made for three different magnitudes of the streamwise thermal-gradient ($\triangle T = 4$, 10 and 18 K), using three different types of aerosols (sodium chloride, ammonium sulfate and sucrose) are going to be evaluated.

2 Theory

2.1 Activation of cloud droplets

The importance of CCN for the formation of cloud droplets is described in the following sections. First, the formation of pure water droplets (homogenous nucleation) is discussed. As will be seen, it is very unlikely for pure water droplets to form and grow into cloud droplets due to their unstable equilibrium with the environment. Much higher ambient super saturations are also required than what is normally found in the atmosphere. Instead, water vapor condenses onto aerosols (working as CCN), to be able to grow into cloud droplets at ambient super saturations. This process, known as heterogenous nucleation, is described in the following section.

2.1.1 Homogenous nucleation

The formation of pure water droplets is called *homogenous nucleation*. This very unlikely process starts off with collisions of water vapor molecules to form intact embryonic water droplets. Work is needed to create the surface area of a droplet, and the net energy increase of the system is found from [1]:

$$\triangle E = A\sigma_w - nVkT \ln \frac{e}{e_{sat}} \tag{1}$$

where $A(= 4\pi R^2)$ and $V(= \frac{4}{3}\pi R^3)$ are the area and volume of the droplet, σ_w is the surface tension of water, n describes the number of moles water molecules the droplet consists of, k is *Boltzmann's constant*, e and T are the vapor pressure and temperature of the system and e_{sat} is the saturation vapor pressure over a plane surface of water of temperature T.

From equation 1 it is seen that the energy of the system is increased for all sub saturated conditions ($e<e_{sat}$). Since a system always strives to achieve lowest possible energy, homogenous nucleation is extremely unlikely under these conditions. However, during super saturated conditions ($e>e_{sat}$), the energy only increases as the radius increases until a certain radius of $R = r$ is reached. Past this point, the energy of the system decreases as the radius of the droplet keeps on increasing. Hence, if a droplet is able to resist evaporation and grow past a radius of r, the water droplet will continue to grow spontaneously to form a cloud droplet. The value for r for a given super saturation can be calculated from *the Kelvin equation* [1]:

$$r = \frac{2\sigma_w}{nkT \ln \frac{e}{e_{sat}}} \tag{2}$$

Another (and more common) way to express the Kelvin equation is shown in equation 3 [2]. Here M_w is the molar mass of water, R is the universal gas constant, ρ_w is the density of water, and D is the droplet diameter.

$$\frac{e}{e_{sat}} = \exp \frac{4M_w\sigma_w}{RT\rho_w D} \tag{3}$$

The vapor pressure adjacent to a droplet always exceeds that adjacent to a plane surface of the same substance [2]. This results from the fact that the attractive forces between molecules at curved surfaces are weaker than those at plane surfaces. Hence, droplets require higher vapor pressures than plane surfaces to keep water molecules from evaporating. The smaller the diameter of a droplet is, the weaker are the attractive forces and the higher becomes the vapor pressure. Thus, smaller droplets require higher ambient super saturations to be in equilibrium with the environment.

The equilibrium of pure water droplets with the environment is very unstable [2]. If a droplet in equilibrium were to collide with a few molecules of water vapor, its diameter would increase (if only infinitesimally) and the vapor pressure of the droplet decrease. Since the partial water pressure of the ambient air stays the same, the vapor pressure of the droplet would become lower than that of the surrounding. More water vapor are then condensed onto the droplet, which grows further and obtains an even lower vapor pressure. In a similar manner, if a few water molecules were to evaporate from a droplet in equilibrium with the environment, the decreased diameter would result in a higher vapor pressure and continued evaporation.

From equation 3, it is found that a droplet of 1 nm requires a super saturation of 721% to be in equilibrium with the environment. However, the real atmosphere rarely obtains a super saturation higher than a few percents [1]. Hence, natural clouds do not consist of droplets formed by homogenous nucleation. Instead, the droplets observed in natural clouds are formed by condensation on atmospheric aerosols. This process is known as *heterogenous nucleation*.

2.1.2 Heterogenous nucleation

The atmosphere is filled with aerosols of different sizes and characteristics. Water vapor is able to condense on particles that are considered to be *wettable*. A particle is perfectly wettable (hydrophilic) if water spreads out as a horizontal film on its surface, and completely unwettable (hydrophobic) if spherical droplets are formed [1]. The same amount of water vapor forms larger droplets when condensed onto atmospheric aerosols than when forming pure water droplets. The droplets then become in equilibrium with the ambient air at lower supersaturations, and it is even possible for growth into cloud droplets at atmospheric super saturations [1]. The aerosols have then served as cloud condensation nuclei (CCN).

Some of the aerosols, upon which water vapor condenses, solute in the water to form solution droplets. This results in a reduction of the water vapor pressure according to *Raoult's law* [1]:

$$\frac{e'}{e_{sat}} = \left[1 + \frac{im_s M_w}{M_s(\frac{\pi}{6}D^3\rho' - m_s)}\right]^{-1} \tag{4}$$

where e' is the saturation vapor pressure adjacent to the solution droplet, m_s is the mass of the dissolved material, ρ' is the density of the solution, M_s is the molecular mass of the dissolved material and i is the van't Hoff factor. For an ideal solution, the van't Hoff factor equals the stoichiometric

dissociation number (the number of ions a molecule dissociates into). However, due to solution non-idealities, the van't Hoff factor usually deviates from this number [3] and calculations of the van't Hoff factor becomes necessary. For the calculations used in this study, see Appendix A.

From equation 4, it can be seen that the vapor pressure depression is enhanced by an increased concentration of the solute. This means that droplets of higher solute concentrations can be in equilibrium with the environment at lower super saturations.

Kelvin's equation and Raoult's law are combined to describe the saturation vapor pressure adjacent to a solution droplet of diameter D_p [3]:

$$\frac{e'}{e_{sat}} = \exp\left[\frac{4M_w\sigma'}{RT\rho_w D_p} - \frac{im_s M_w}{M_s(\frac{\pi}{6}D_p^3\rho' - m_s)}\right] \tag{5}$$

The contribution of the solute to the total mass can often be neglected [2], simplifying equation 15 to:

$$\frac{e'}{e_{sat}} = \exp\left[\frac{4M_w\sigma'}{RT\rho_w D_p} - \frac{6im_s M_w}{M_s\pi D_p^3\rho'}\right] \tag{6}$$

Setting:

$$A = \frac{4M_w\sigma'}{RT\rho_w}$$

$$B = \frac{6im_s M_w}{M_s\pi\rho'}$$

equation 6 can also be expressed as:

$$\ln\left(\frac{e'}{e_{sat}}\right) = \frac{A}{D_p} - \frac{B}{D_p^3} \tag{7}$$

Equation 5, 6 and 7 are different ways of expressing the so called *Köhler equation*. The first expression on the r.h.s (A/D_p) is called the *curvature term* and the second expression (B/D_p^3) is referred to as the *solute effect term* [2]. As described earlier, the curvature term works to increase the vapor pressure of the droplet while the solute effect works to decrease it. It can be seen that both effects increase with decreasing droplet size. However, the solute effect increases much faster and Raoult's law dominates therefore for small droplet diameters. As the droplets grow larger, the Kelvin curvature effect takes over [1]. This is expected considering that the amount of solute stays fixed, resulting in the droplets becoming more and more like pure water droplets as they grow.

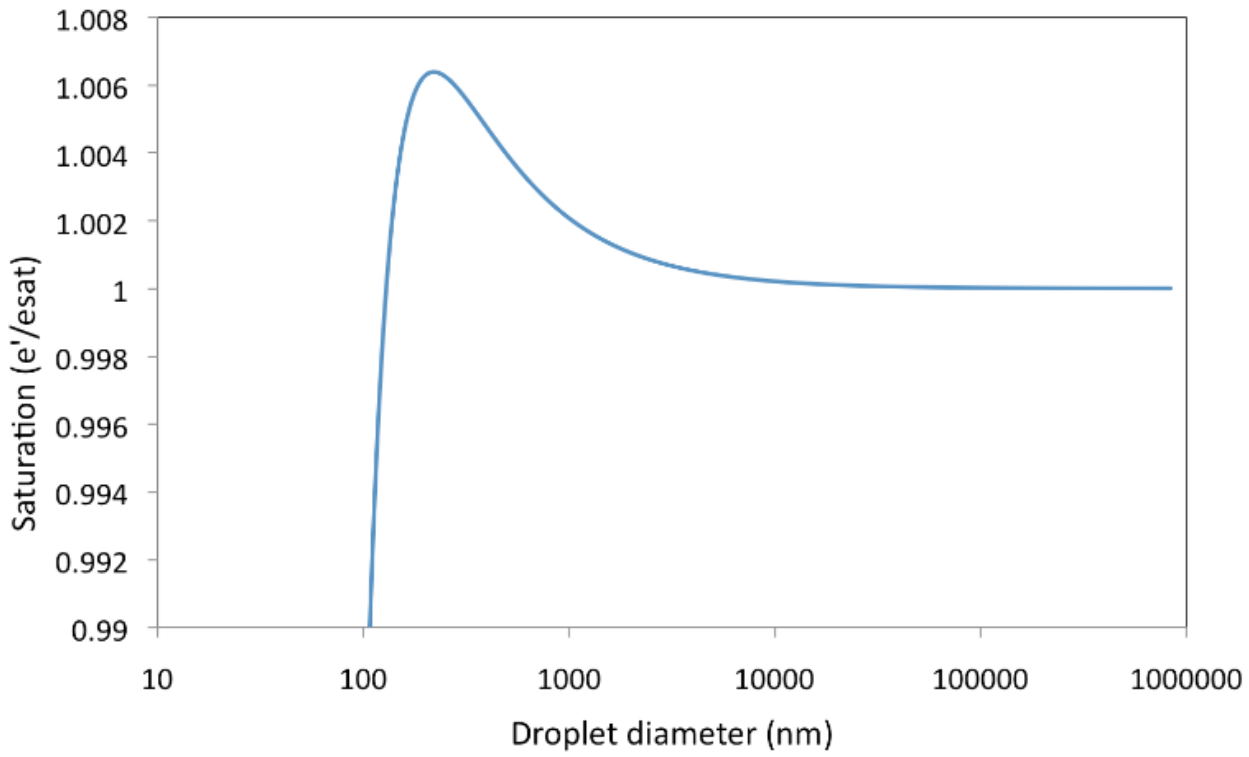

Figure 1: Köhler curve for a sodium chloride particle with a dry diameter of 30 nm.

When the saturation ratio (or super saturation) adjacent to a solution droplet is plotted against the droplet's diameter, a so called *Köhler curve* is obtained [1]. An example of a Köhler curve is shown in figure 1.

The characteristic maximum of the Köhler curve corresponds to the critical saturation ratio S_c:

$$\ln S_c = \left(\frac{4A^3}{27B}\right)^{1/2} \tag{8}$$

which is reached at the critical droplet diameter D_{pc}:

$$D_{pc} = \left(\frac{3B}{A}\right)^{1/2} \tag{9}$$

The dependence of the particle dry diameter (d_0) on the critical saturation ratio is illustrated in figure 2.

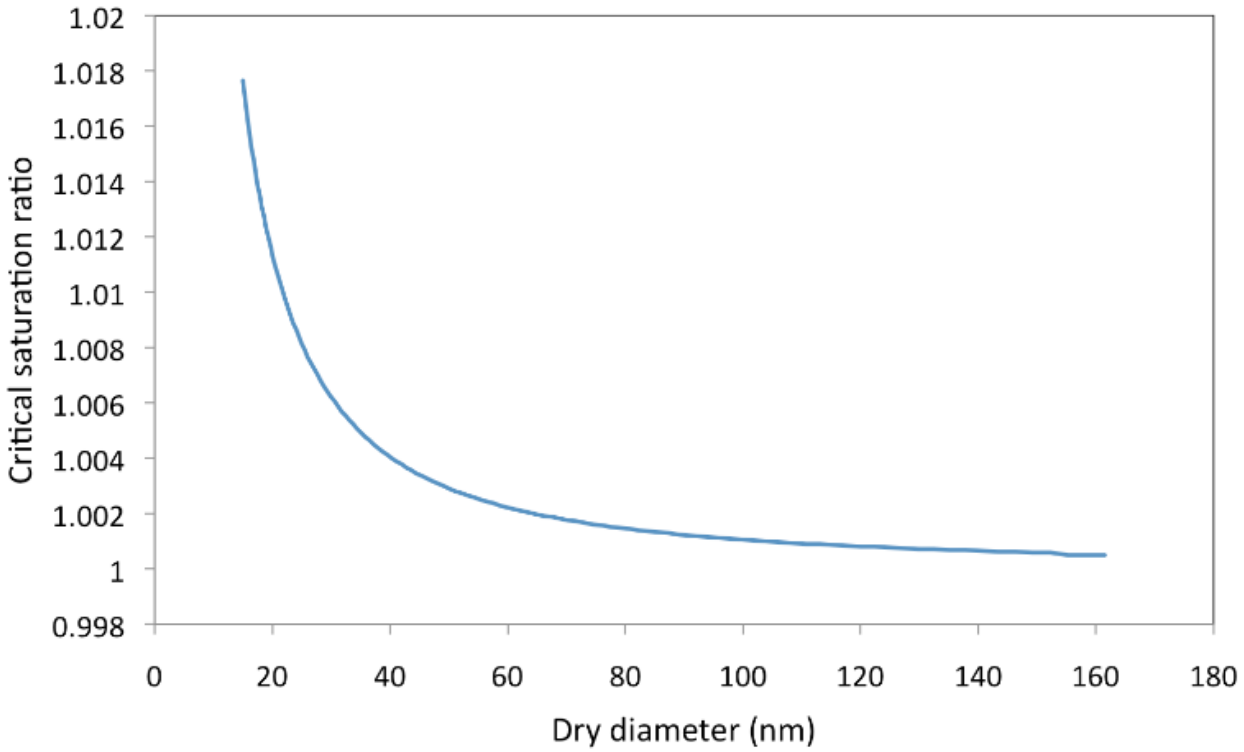

Figure 2: Critical saturation ratio as a function of dry diameter for sodium chloride particles.

The Köhler curve represents the equilibrium sizes of droplets for different environmental saturations [2]. If the equilibrium size of a droplet is less than D_{pc}, the droplet is in stable equilibrium with the environment. If the size of the droplet were to become slightly larger than this size, its equilibrium vapor pressure would become larger than the saturation of the environment, causing water molecules to evaporate from the droplet until equilibrium once again was reached. If the droplet instead were to loose a couple of water molecules, its equilibrium vapor pressure would decrease, causing water vapor to condense onto the droplet until equilibrium was reached. However, if the equilibrium diameter is larger than D_{pc}, a small growth of the droplet would cause its equilibrium vapor pressure to become smaller than the saturation of the environment, and the droplet would continue to grow uncontrollably. In a similar manner, evaporation of the droplet would lead to continued evaporation. Hence, droplets with diameters larger than D_{pc} are in unstable equilibrium with the environment.

A droplet with a diameter smaller than D_{pc} is only able to grow past its critical diameter when the ambient saturation ratio is greater than S_c. The droplet is then said to be activated and continues to grow spontaneously [2]. It is first in this stage that the droplet is considered to be a cloud droplet. Due to diffusional kinetics and the availability of water vapor, the growth is usually limited to about 10 μm [4].

2.2 Instrument description

2.2.1 The cloud condensation nuclei counter

For this study, the Continuous-Flow Streamwise Thermal-Graident Cloud Condensation Nuclei Counter from Droplet Measurement Technologies (CCNC DMT-100) was used (figure 3). The CCNC consists of a vertically mounted 50 cm high cylindrical column with wetted inner walls and a linear temperature gradient in the streamwise direction [5]. The magnitude of the temperature gradient is controlled by three thermoelectric coolers which are attached at the beginning, middle and end of the outer wall of the column [5]. Both the water vapor and the heat of the inner walls diffuse in the radial direction towards the center of the column. Due to the fact that water vapor diffuses faster than heat, the centerline becomes super saturated (for further explanation, see section 2.2.3).

The aerosol sample enters the centerline of the column from the top and is surrounded by humidified filtered sheath air. The recommended flow ratio between sample and sheath air is 1 to 10 [5]. If the super saturation of the centerline is larger than the critical super saturation (SS_c) of the aerosols, the aerosols become activated [6]. The activated nuclei are counted and sized by an optical particle counter (OPC) into 20 different size bins. The OPC consists of a 35 mW, 660 nm wavelength diod laser and is able to measure particles of the size range 0.75 - 10 μm [5].

Figure 3: The Continuous-Flow Streamwise Thermal-Graident Cloud Condensation Nuclei Counter from Droplet Measurement Technologies (CCNC DMT-100) [5].

2.2.2 Theory of operation

The CCNC operates on the principle that water vapor diffuses faster than heat [5]. The time it takes for the water vapor and heat of the inner walls to reach the centerline of the column can be calculated from:

$$\tau_C = \frac{R^2}{D_v} \tag{10}$$

$$\tau_T = \frac{R^2}{\alpha} \tag{11}$$

respectively, where R is the radius of the column, D_v is the diffusivity of water vapor and α is the diffusivity of heat [4]. Knowing that $D_v > \alpha$, it is seen that $\tau_C < \tau_T$. Hence, it will take a longer time for the heat to reach the centerline than for the water vapor.

The mean velocity of the flow in the column is given by:

$$V = \frac{Q}{\pi R^2} \tag{12}$$

where Q is the flow rate. This means that the water vapor and heat will travel an axial distance of:

$$x_C = V\tau_C = \frac{Q}{\pi D_v} \tag{13}$$

$$x_T = V\tau_T = \frac{Q}{\pi \alpha} \tag{14}$$

respectively, before reaching the centerline. Since, the heat travels a longer axial distance before reaching the centerline, the heat at a certain position of the centerline must originate from a higher level than the water vapor of the same position. Since the temperature decreases in the anti-streamwise direction, the temperature surrounding the water vapor at the centerline must be lower than the temperature originally surrounding the water vapor at the column wall. Assuming that the water vapor was saturated at the column wall, the centerline must become super saturated [5]. Since the water vapor and temperature gradients are constant along the wetted wall, the super saturation of the centerline is uniform at a given point in time [5]. The magnitude of the super saturation depends on the flow rate (Q), pressure (P), sample temperature (T_{sample}) and streamwise temperature gradient($\triangle T$) of the column [3].

2.2.3 The scanning flow CCN analysis (SFCA)

Previously, the CCNC operated in a so called *Continuous-Flow Streamwise Thermal-Gradient* (CF-STGC) operation mode. In this operation mode, the super saturation of the centerline is altered by changing $\triangle T$ in a stepping manner while Q and P are kept constant. However, this operation mode has some limitations. First of all, it takes about 20 to 40 seconds for the column temperatures to stabilize (and sometimes up to 3 minutes for the OPC temperature) after the value of $\triangle T$ has been altered [6]. Due to the slow temperature stabilization, a lot of valuable information can get lost (especially at field measurements of highly heterogenous air) at the same time as the measurements usually become limited to just a single or a few super saturations at a time [6]. Second of all, the varied temperature difference also makes it possible for some organic-rich aerosols to partially volatilize in the CCNC, which of course, affects the measurements [6]. To minimize volatilization biases and at the same time obtain much faster measurements of entire super saturation spectra, Moore and Nenes developed the *Scanning Flow CCN Analysis* (SFCA).

The SFCA works to vary the super saturation of the column by continuously changing the flow rate while keeping P and $\triangle T$ constant. The flow rate of the CCNC is linearly decreased from a maximum flow rate of Q_{max} to a minimum flow rate of Q_{min} over a ramp time t_{down}. The minimum flow rate is then held constant for t_{base} before the flow rate is linearly increased from Q_{min} to Q_{max} over a ramp time t_{up}. The maximum flow rate is then held constant for t_{peak} before the cycle starts over. If the time of flow change (t_{up} or t_{down}) is much larger than the diffusivity time scale (τ_C and τ_T) a quasi steady super saturation develops at the centerline [6]. This quasi steady super saturation is linearly dependent on the flow rate, resulting in a linear variation of the super saturation with time. Hence, the SFCA enables high temporal measurements of entire super saturation spectra. Fast and continuous measurements are essential when studying rapidly aging aerosols, as well as small samples and fast processes. Since the measurement operates at a single $\triangle T$, biases from partial volatilization are also minimized [6].

In this study, the instantaneous flow rates of the CCNC are converted into the corresponding super saturations of the instrument. This is done by examining the flow rates at which particles of known sizes and characteristics activate into cloud droplets. The critical flow rates can then be related to the critical super saturations of the particles found from Köhler theory. In this way, calibrations between the flow rates and super saturations of the CCNC are obtained. However, it is crucial to use the same scan times for the calibrations as for the measurements when the ramp times (t_{up} and t_{down}) are shorter than 600 s. The super saturations obtained for these ramp times are namely larger for down-scans than for up-scans [6]. However, evaluation of down-scans lay beyond the scope of this study. In this study, only up-scans are evaluated.

3 Method

In this calibration study, the activation of three different types of aerosols were examined, namely sodium chloride, ammonium sulfate and sucrose. The aerosols were generated by nebulization of aqueous solutions using an atomizer. To make sure that the generated particles were dry, the aerosols were mixed with particle-free dry air to obtain a relative humidity of less than 10 %. The aerosols were then passed through two radioactive neutralizers. The object of the radioactive neutralizers were to establish charge equilibrium in the aerosols, so that specific sizes could be chosen by the differential mobility analyzer (DMA) [3]. The DMA chooses the desired aerosol sizes by varying its flow rate and electric field [4]. Part of the sample air then continues to a condensation particle counter (CPC), where the raw particle concentration was counted, while the rest continued to the cloud condensation nuclei counter (CCNC) and mass flow controller (MFC). The flow rate through the CCNC is regulated between Q_{min} and Q_{max} by an internal pump. The MFC is used to compensate for the flow variations in the CCNC and thereby keeping the total aerosol flow constant. For this study, Q_{min} and Q_{max} were set to 200 cm^3/min and 1000 cm^3/min respectively, t_{peak} and t_{base} were set to 25 s and t_{up} and t_{down} to 125 s. All measurements were performed at room temperature and standard pressure. The experimental setup is illustrated in figure 4.

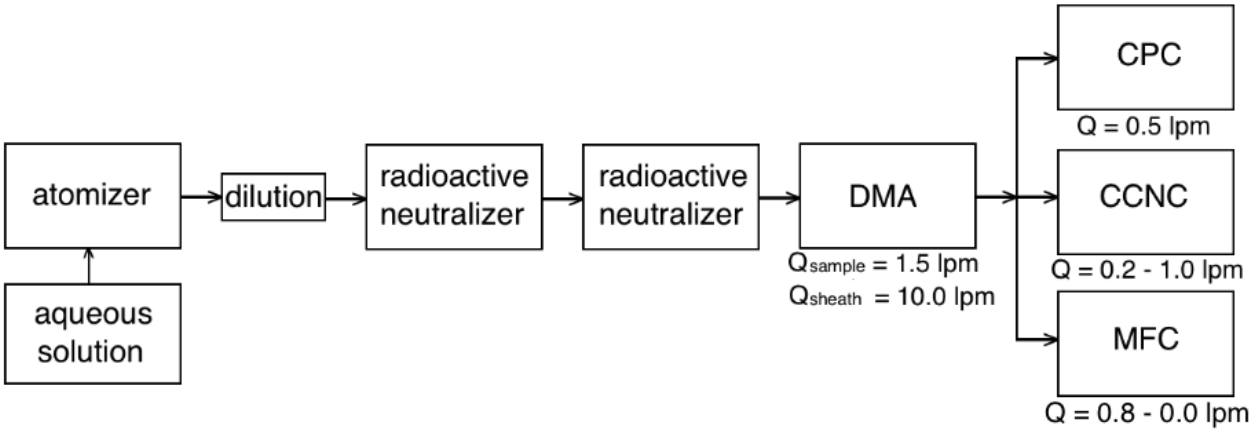

Figure 4: Illustration of the experimental setup: DMA - differential mobility analyzer, CPC - condensation particle counter, CCNC - cloud condensation nuclei counter, MFC - mass flow controller.

The critical flow rates of the substances were examined for three different values of $\triangle T$ (4, 10 and 18 K) as a function of dry diameter (d_o). For a given substance and $\triangle T$, 11 different diameters were chosen by the DMA, where each diameter would run for two cycles before switching to the next. Each cycle lasted for 285 s, followed by a diameter switch of 30 s. The diameters were set to change during down scans so that the up scans wouldn't be affected by the diameter switch and could safely be used for evaluation. However, a slight deviation of approximately one second in the DMA caused the diameter switch to affect the up scans in the long run. These up scans were not evaluated.

In an ideal measurement, the CCN number concentration should start off as zero ($N_{CCN}/N_{CN} = 0$) since the low flow rates correspond to super saturations lower than the critical super saturation

of the particles. After the critical flow rate has been reached, the CCN number concentration should equal the total particle concentration ($N_{CCN}/N_{CN} = 1$), corresponding to an activation of all particles. The activation curve should thereby take the form of a step function. However, due to limitations in the DMA's particle size resolution, slightly smaller and larger particles than the selected sizes were also included in the measurements [3]. Activation would therefore take place at slightly different flow rates depending on the variation of diameters in the measurement. Hence, a more gradual increase from $N_{CCN}/N_{CN} = 0$ to $N_{CCN}/N_{CN} = 1$ was obtained.

The critical flow rate, Q_{50}, of a measurement was taken as the value where 50% of the particle concentration had activated to CCN. This value was found by fitting sigmoidal activation curves to the measurements in MATLAB. When fitting the curves, the plateaus at the lower flow rates had to been taken into account. These plateaus correspond to the activation of doubly charged particles. The DMA believes that these particles are of the same size as the singly charged particles, but in reality, they are larger and are therefore activated at lower super saturations. When deciding on the critical flow rate for the singly charged particles, the plateau is therefore taken as the lower level ($N_{CCN}/N_{CN} = 0$). A typical activation curve is shown in figure 5.

The diameters set for the DMA to choose did not exactly correspond to the chosen diameters. This offset was caused by a deviation of the voltage read by the DMA from the actual voltage of the instrument. Using a voltmeter to measure the actual voltage of the DMA and comparing these values with the voltages belonging to the selected diameters, a calibration was made. The diameters set for the DMA could then be converted to the actual diameters of the chosen particles.

Between 9 and 22 critical flow rates were recorded for each diameter. The critical super saturation for each diameter was calculated using Köhler theory (see Appendix A). The measured flow rates could in this way be related to the super saturations of the CCNC. A linear calibration between the super saturations and flow rates was made for each substance and $\triangle T$, giving nine calibration curves in total. To verify the validity of the curves, a 95% confidence interval was also calculated. For the linear calibrations and confidence interval calculations, see Appendix B.

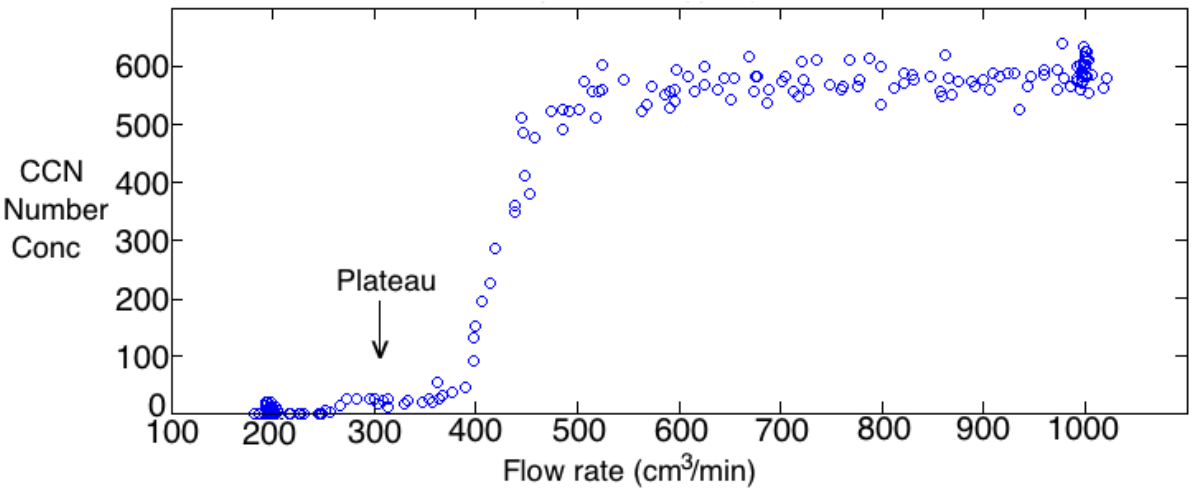

Figure 5: Illustration of an activation curve for a sodium chloride particle of 40 nm at $\triangle T = 10$ K. The plateau at the lower flow rates corresponds to the activation of doubly charged particles.

4 Results

The calibration curves obtained by sodium chloride, ammonium sulfate and sucrose can be viewed in figures 6, 7 and 8, respectively. A 95% confidence interval is displayed for each curve, as well as the measured data used to construct the curves. As expected, the super saturations of the CCNC increases with an increasing streamwise temperature gradient. It can further be seen that a range of super saturations can be obtained from more than one temperature gradient. For example, the calibrations made by sodium chloride shows that a super saturation of 0.4% can be obtained by the combination of a 4 K temperature gradient and a flow rate of 1000 cm^3/min, but also for a temperature gradient of 18 K and a flow rate of 220 cm^3/min.

From figures 6, 7 and 8, it can also be seen that the spread of the measured data increases with an increasing temperature gradient. A particular big spread is found for the highest flow rates of the calibrations made by sodium chloride and ammonium sulfate for a temperature gradient of 18 K. The spread of the data obtained by sucrose isn't nearly as large for this temperature gradient. For all curves, the measurements corresponding to the lowest and highest flow rates are positioned slightly under the calibration curve, while the measurements corresponding to the intermediate flow rates are placed slightly above. It can also be seen that the measurements only correspond to a range of the flow rates. No measurement equals a flow rate below 250 cm^3/min or above 850 cm^3/min.

The magnitude of the confidence intervals for the streamwise temperature gradients of 4, 10 and 18 K are visualized in tables 1, 2 and 3, respectively. It is clear that the 95% confidence intervals become larger as the streamwise temperature difference increses. It can also be seen that the confidence intervals are the largest for the ends of the calibration curves, where the highest interval always is presented by the end corresponding to the highest flow rate. However, there is no direct trend regarding the magnitude of the 95% confidence intervals between the substances. For example, sodium chloride presents the largest intervals for $\triangle T = 18$ K and the smallest intervals for $\triangle T = 10$ K, while its values are nearly identical to those obtained by sucrose for $\triangle T = 4$ K.

The calibration curves found for the streamwise temperature gradients of 4, 10 and 18 K are plotted together in figures 9, 10 and 11, respectively. As can be seen from the figures, the calibration curves found from the different substances are not consistent. It can be seen that sodium chloride always predicts the lowest super saturations for the given flow rates while sucrose predicts the highest (except at the lowest flow rates of $\triangle T$=18 K, where ammonium sulfate predicts higher super saturations than sucrose). Furthermore, the slope of the calibration curves are almost identical for $\triangle T = 4$ and 10 K, while a deviation exist between the slopes of the curves for $\triangle T = 18$ K.

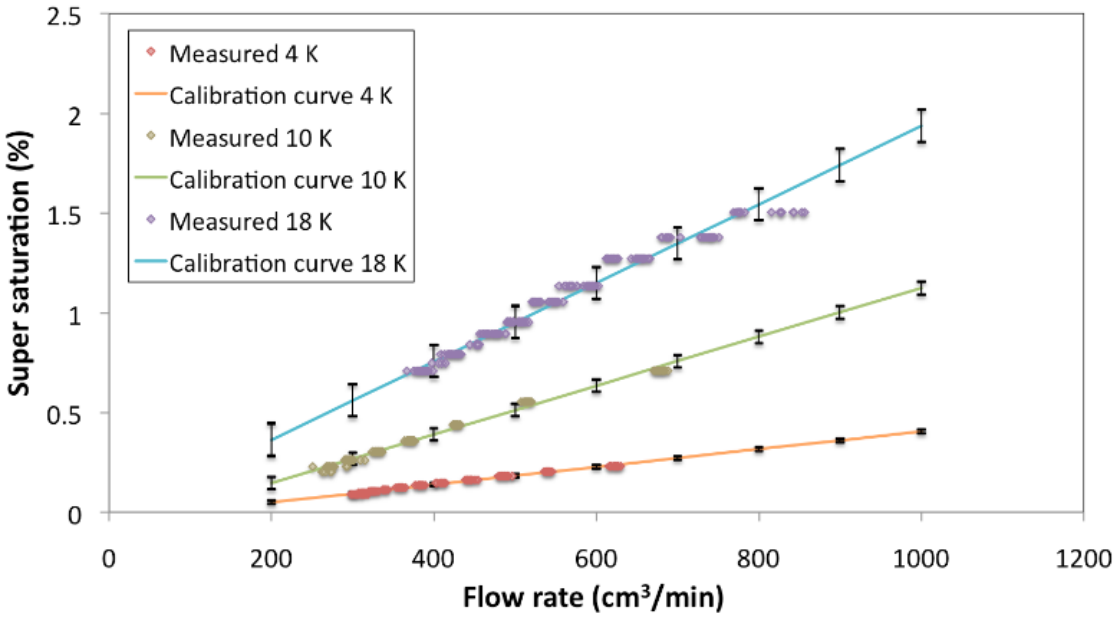

Figure 6: Calibration curves and 95% confidence intervals obtained by sodium chloride for streamwise temperature gradients of 4 K (orange line), 10 K (green line) and 18 K (blue line). The measured data used to create the calibration curves are displayed with diamonds of corresponding color.

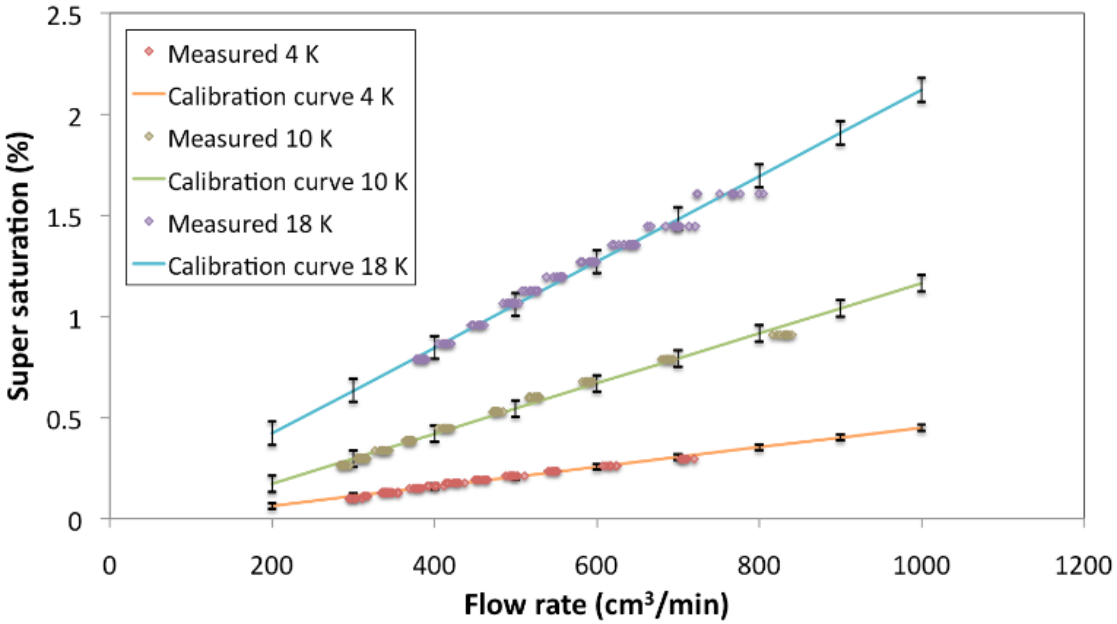

Figure 7: Calibration curves and 95% confidence intervals obtained by ammonium sulfate for streamwise temperature gradients of 4 K (orange line), 10 K (green line) and 18 K (blue line). The measured data used to create the calibration curves are displayed with diamonds of corresponding color.

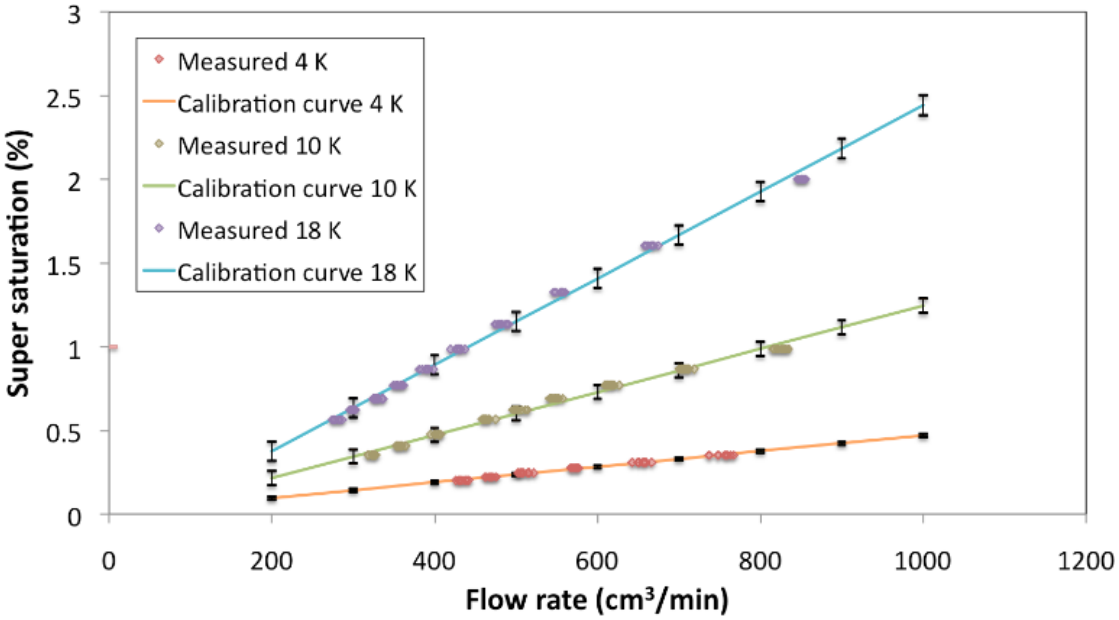

Figure 8: Calibration curves and 95% confidence intervals obtained by sucrose for streamwise temperature gradients of 4 K (orange line), 10 K (green line) and 18 K (blue line). The measured data used to create the calibration curves are displayed with diamonds of corresponding color.

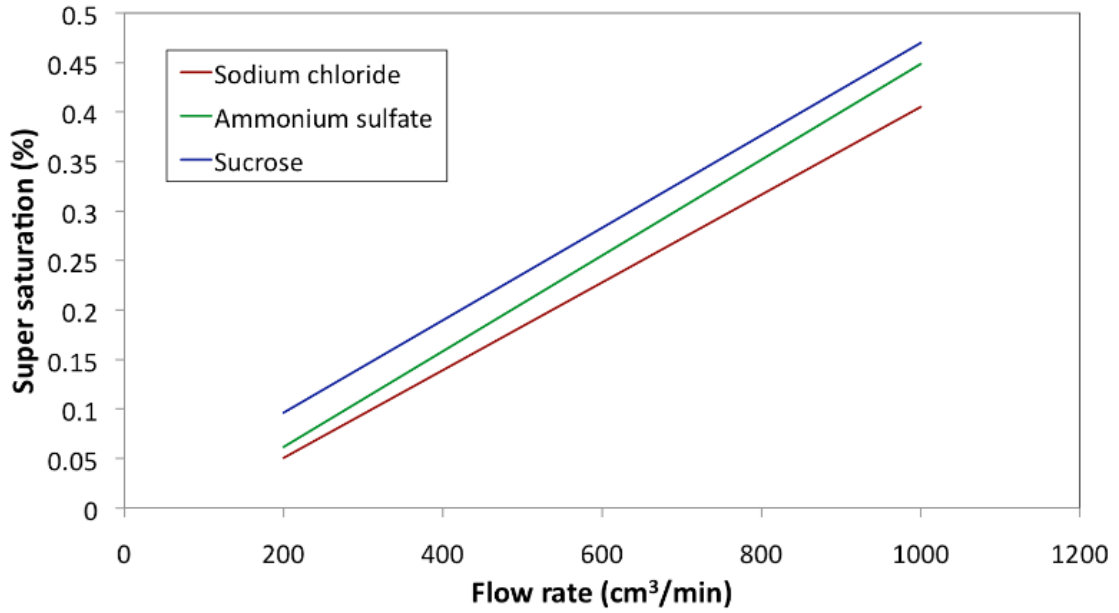

Figure 9: Calibration curves obtained for a streamwise temperature difference of 4 K by calibration of sodium chloride (red, y=0.00044x-0.0378), ammonium sulfate (green, y=0.00048x-0.0348) and sucrose (blue, y=0.00047x+0.0032).

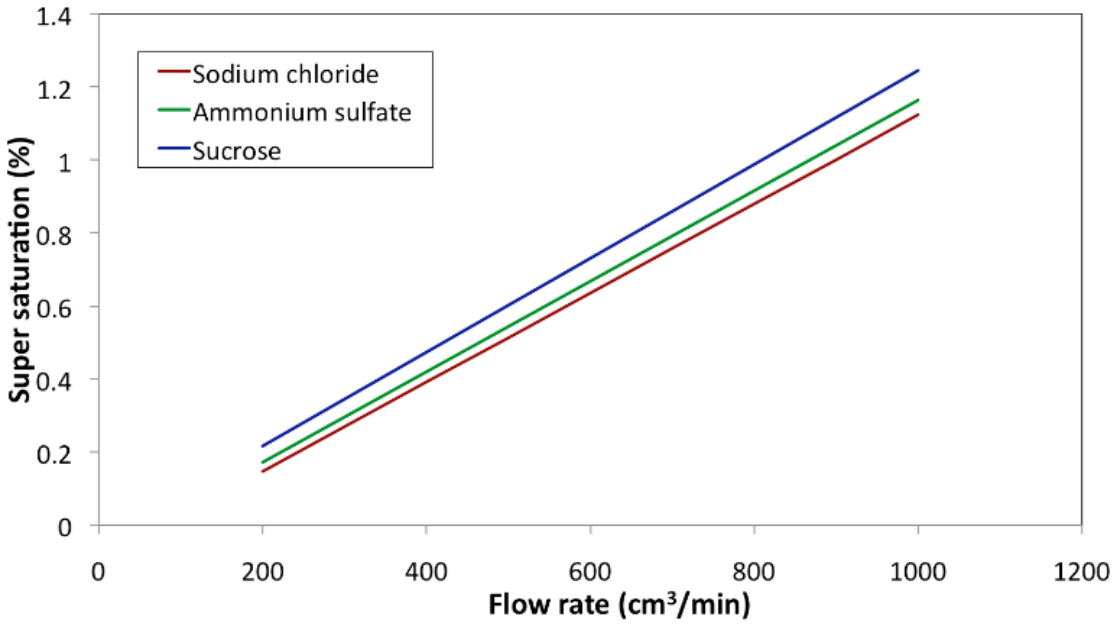

Figure 10: Calibration curves obtained for a streamwise temperature difference of 10 K by calibration of sodium chloride (red, y=0.00122x-0.0979), ammonium sulfate (green, y=0.00124x-0.0764) and sucrose (blue, y=0.00129x-0.0411).

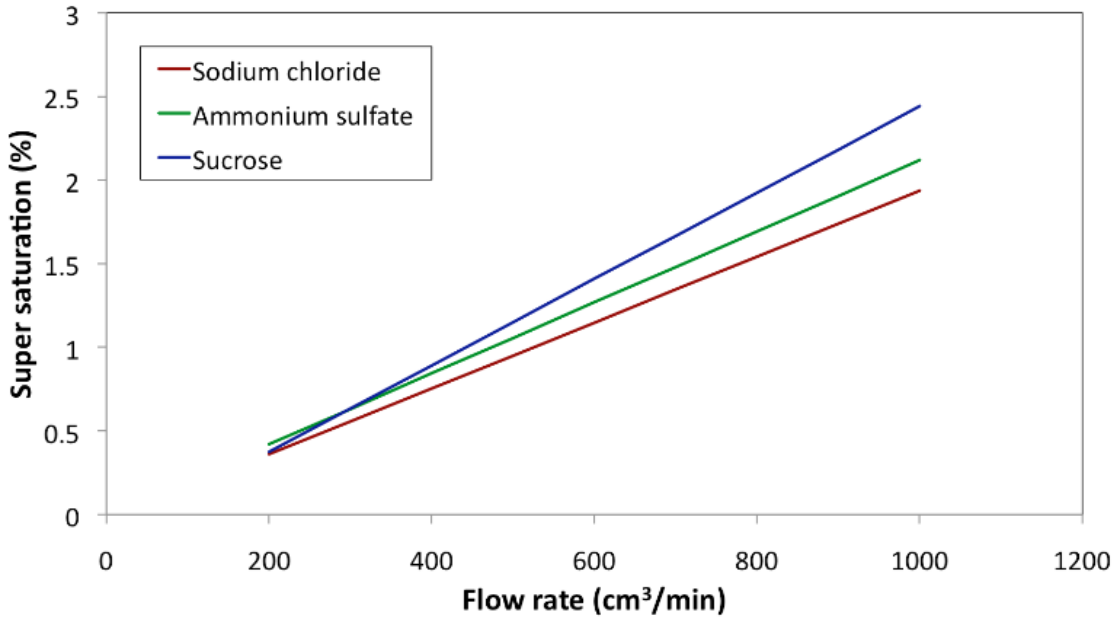

Figure 11: Calibration curves obtained for a streamwise temperature difference of 18 K by calibration of sodium chloride (red, y=0.00197x-0.0316), ammonium sulfate (green, y=0.00212x-0.0028) and sucrose (blue, y=0.00258x-0.1406).

Flow (cm^3/min)	95% confidence interval (percentage points) Sodium chloride	Ammonium sulfate	Sucrose
200	±0.0089	±0.0145	±0.0095
300	±0.0088	±0.0143	±0.0092
400	±0.0087	±0.0142	±0.0090
500	±0.0088	±0.0142	±0.0088
600	±0.0088	±0.0143	±0.0088
700	±0.0090	±0.0144	±0.0089
800	±0.0092	±0.0146	±0.0091
900	±0.0094	±0.0149	±0.0094
1000	±0.0097	±0.0153	±0.0098

Table 1: The 95% confidence intervals for the calibration curves obtained by sodium chloride, ammonium sulfate and sucrose for a streamwise temperature difference of 4 K. The confidence intervals are given as percentage points of the super saturation value for the corresponding flow rate. For example, ±0.0089 for a flow rate of 200 cm^3/min for sodium chloride refers to a super saturation of $0.0508\% \pm 0.0089$ percentage points.

Flow (cm^3/min)	95% confidence interval (percentage points) Sodium chloride	Ammonium sulfate	Sucrose
200	±0.0311	±0.0406	±0.0423
300	±0.0309	±0.0404	±0.0419
400	±0.0309	±0.0403	±0.0416
500	±0.0309	±0.0403	±0.0415
600	±0.0311	±0.0403	±0.0415
700	±0.0313	±0.0405	±0.0417
800	±0.0317	±0.0407	±0.0420
900	±0.0322	±0.0407	±0.0425
1000	±0.0327	±0.0414	±0.0431

Table 2: The 95% confidence intervals for the calibration curves obtained by sodium chloride, ammonium sulfate and sucrose for a streamwise temperature difference of 10 K. The confidence intervals are given as percentage points of the super saturation value for the corresponding flow rate. For example, ±0.0311 for a flow rate of 200 cm^3/min for sodium chloride refers to a super saturation of $0.1465\% \pm 0.0311$ percentage points.

Flow (cm^3/min)	95% confidence interval (percentage points) Sodium chloride	Ammonium sulfate	Sucrose
200	±0.0813	±0.0579	±0.0576
300	±0.0807	±0.0570	±0.0572
400	±0.0802	±0.0564	±0.0569
500	±0.0800	±0.0561	±0.0569
600	±0.0800	±0.0561	±0.0571
700	±0.0802	±0.0564	±0.0575
800	±0.0806	±0.0570	±0.0581
900	±0.0813	±0.0578	±0.0588
1000	±0.0821	±0.0590	±0.0598

Table 3: The 95% confidence intervals for the calibration curves obtained by sodium chloride, ammonium sulfate and sucrose for a streamwise temperature difference of 18 K. The confidence intervals are given as percentage points of the super saturation value for the corresponding flow rate. For example, ±0.0813 for a flow rate of 200 cm^3/min for sodium chloride refers to a super saturation of $0.3620\% \pm 0.0813$ percentage points.

5 Discussion

5.1 Comparison of calibration curves obtained by the same substance

The super saturations of the CCNC increases with an enhanced streamwise temperature gradient. The larger the super saturations of the CCNC are, the smaller particles are needed for calibration. However, small particles are very sensitive to deviations of the DMA voltage. A deviation of just a few volts will cause the wrong diameter to be chosen for particles around 20 nm, while the voltage is required to change with about 20 volts for the wrong particle size to be chosen for diameters around 150 nm (see Appendix C). Hence, larger uncertainties are associated with the particle sizes for the calibrations of $\triangle T = 18$ K than $\triangle T = 10$ and 4 K. From figure 2 it can also be seen that the magnitude of the critical super saturation increases exponentially with a decreasing diameter. It is therefore of no surprise that the largest confidence intervals are found for the streamwise temperature gradient of 18 K.

However, from figures 6-8, it can be seen that some diameters were used to calibrate more than one value of $\triangle T$ (same value of SS_c for different $\triangle T$). The 95% confidence intervals corresponding to the same diameter of the same substance are expected to be the same. However, tables 1-3 show a significant increase of the 95% confidence intervals with an increasing temperature gradient. This leads to the assumption that there is something in the CCNC which also contributes to the larger uncertainties of the calibration curves made for a streamwise temperature gradient of 18 K.

5.2 Comparison of calibration curves obtained for the same $\triangle T$

The calibration curves found for the same values of $\triangle T$ are not consistent. From figures 9-11, it can be seen that sodium chloride always predicts the lowest super saturations while sucrose predicts the highest (except at the lowest flow rates of $\triangle T$=18 K, where ammonium sulfate predicts higher super saturations than sucrose). This displacement in y-direction may be caused by an offset in the DMA voltage as well as an assumption that the chosen particles are spherical.

The DMA voltages measured at the beginning of the study did not correspond to the voltages measured at the end (see Appendix C). Since the voltages measured at the beginning of the study were used for all diameter calibrations, some diameters were found to be smaller than their actual size. Hence, larger super saturations were obtained from the Köhler calculations for these measurements than the actual super saturations of the CCNC. Given that the switch from the initial to the final voltages were continuous, a gradual increase of the super saturations should be found. This is almost what was found, where the order of measurements were sodium chloride 4 K, 10 K, 18 K, ammonium sulfate 18 K, 10 K, sucrose 18 K, 10 K, 4 K and ammonium sulfate 4 K. Since ammonium sulfate 4 K was the absolute last measurement, a continuous change of the DMA voltage cannot be the entire explanation for the inconsistency. Whether or not the voltage switch of the DMA actually was continuous also remains uncertain. It is most likely only the measurements of sucrose 18 K, 10 K, 4 K and ammonium sulfate 4 K that were affected by the voltage switch, since the instrument was temporarily turned off prior to these measurements. In previous studies, the voltages of the DMA have stayed rather constant [10].

When choosing particle sizes, the DMA assumes perfectly spherical particles. However, particles of sodium chloride have an almost cubic shape and particles of ammonium sulfate also deviates from a fully spherical shape [3]. For these particles, the mobility equivalent diameters selected by the DMA are larger than their mass equivalent diameters [3]. This means that larger diameters were used for the Köhler calculations than the actual sizes of the particles (given that the DMA calibration was correct). To correct for the shape, so called shape factors can be included in the Köhler calculations. A shape factor of 1.08 is recommended for sodium chloride and 1.02 for ammonium sulfate [3]. Hence, the calibration curves obtained for sodium chloride and ammonium sulfate should be shifted towards higher super saturations. Since sodium chloride deviates the most from a perfectly spherical shape, the shift should be the largest for this curve. However, it remains uncertain whether or not a shape factor should be included in the calculations of sucrose.

Of the calibration curves obtained for the streamwise temperature difference of 18 K, the one made by sucrose is expected to be the most accurate. Using the equations and variables displayed in Appendix A, it can be shown that particles of sucrose corresponding to a given critical super saturation are larger than the corresponding particles of sodium chloride and ammonium sulfate. For example, a super saturation of 1.5% corresponds to the activation of sucrose particles with dry diameters of 42 nm, while it corresponds to the activation of particles of 22.5 and 17 nm for ammonium sulfate and sodium chloride, respectively. As discussed earlier, calibrations made by larger diameters aren't as sensitive to deviations of the DMA voltage, and are therefore expected to be more accurate. However, the confidence intervals expressed in table 3 shows that the 95% confidence interval is the smallest for sucrose only for a flow rate of 200 cm^3/min. For the remaining flow rates ammonium sulfate represents smaller confidence intervals. This is most likely a result of more measurements being used to construct the calibration curve for ammonium sulfate than sucrose. Hence, to increase the certainty of the sucrose calibration, more measurements have to be made. Due to time limitation, it wasn't possible to make any more measurements for this study.

5.3 Validity of the calibration curves

The measured data displayed in figures 6-8 are not entirely linear. It can be seen that the data points corresponding to the highest and lowest flow rates always are positioned slightly under the calibration curve, while the data points belonging to the intermediate flow rates are positioned slightly above. It is therefore possible that a second order polynomial would have been a better representation of the variation of the super saturation with the flow rate than a linear fit.

From figures 6-8, it can also be seen that no measurement corresponds to a flow rate below 250 cm^3/min or above 850 cm^3/min. This is a result of the difficulty to determine Q_{50} from the sigmoidal fits for these critical flow rates. For critical flow rates beneath 250 cm^3/min, there are no longer any lower levels to make the fits from. In a similar manner, it is very hard to make fits for critical flow rates higher than 850 cm^3/min due to missing upper levels. Hence, the calibration curves are extrapolated towards lower and higher flow rates. It is therefore of no surprise that the largest uncertainties are found for the ends of the calibration curves. For all calibration curves, the largest uncertainties were found for the ends corresponding to the highest flow rates. This is a result of the highest flow rates corresponding to the activation of the smallest particles.

6 Conclusion

Viewed individually, the calibration curves suggest that the SFCA operation mode is reliable. However, the increasing spread of the measured data with an enhanced temperature gradient reveals that the operation mode becomes less reliable as the streamwise thermal gradient becomes higher. For calibrations of high temperature gradients, sucrose is recommended over sodium chloride and ammonium sulfate.

The calibration curves were found to be the least reliable at the ends. No measurement could be made below a flow rate of 250 cm^3/min or above a flow rate of 850 cm^3/min. The super saturations and flow rates of the CCNC were also found to deviate from a completely linear relationship. It is therefore recommended to stay in the calibrated regions when making actual measurements.

From the study, it was also discovered that it is important to check the DMA voltages regularly. Even though the voltages have stayed rather constant in previous studies, they were found to change over time in this study.

References

[1] Wallace, J.M., Hobbs, P.V. (2006) *Atmospheric Science: An Introductory Survey*, 2nd Edition, Academic Press

[2] Senifeld, J.H., Pandis, S.N. (2006) *Atmospheric Chemistry and Physics: From Air Pollution to Climate Change*, 2nd Edition, Wiley-Interscience

[3] Rose, D., Gunthe, S.S., Mikhailov, E., Frank, G.P., Dusek, U., Andreae, M.O., Pschl, U. (2008) Calibration and measurement uncertainties of a continuous-flow cloud condensation nuclei counter (DMT-CCNC): CCN activation of ammonium sulfate and sodium chloride aerosol particles in theory and experiment *Atmos. Chem. Phys.* 8, 1153-1179

[4] Roberts, G.C., Nenes, A. (2005) A Continuous-Flow Streamwise Thermal-Gradient CCN Chamber for Atmospheric Measurements *Aerosol Science and Technology* 39, 206-221

[5] (2012) *Cloud Condensation Nuclei (CCN) Counter - Manual for Single-Column CCNs* DOC-0086 Revision 1-2, Droplet Measurement Technologies, Boulder, CO

[6] Moore, R.H., Nenes, A. (2009) Scanning Flow CCN Analysis - A Method for Fast Measurements of CCN Spectra *Aerosol Science and Technology* 43, 1192-1207

[7] Rosenørn, T., Kiss, G., Bilde, T. (2006) Cloud droplet activation of saccharides and levoglucosan particles *Atmospheric Environment* 40, 1794-1802

[8] Sharaf, M.A., Illman, D.L., Kowalski B.R. (1981) *Chemometrics* vol. 82, John Wiley, New York

[9] Blom, G (1970) *Statistikteori med tillmpningar* Studentlitteratur, Lund

[10] Personal communication with Birgitta Svenningsson

Appendix A

When calculating the the critical super saturations from Köhler theory, the following form of the Köhler equation was used:

$$\frac{e'}{e_{sat}} = \exp\left[\frac{4M_w\sigma'}{RT\rho_w D} - \frac{im_s M_w}{M_s(\frac{\pi}{6}D^3\rho' - m_s)}\right] \tag{15}$$

Due to the small difference between ρ' and ρ_w and between σ' and σ_w for the solution droplets [3], ρ' was set to ρ_w and σ' to σ_w for the calculations.

The mass of the solute, m_s was found from the following relation:

$$m_s = \frac{\pi}{6}d_0^3\rho_d \tag{16}$$

where d_0 is the dry diameter of the solute.

The van't Hoff factor, i, was set to a fixed value of 1 for sucrose [7], while it was set to vary with the droplet size for sodium chloride and ammonium sulfate [3]. The variation of i with the droplet size was calculated from the following expression:

$$i = \frac{1 - \exp\left(-v_s\phi_s\mu_s M_w\right)}{\mu_s M_w \exp\left(-v_s\phi_s\mu_s M_w\right)} \tag{17}$$

where v_s is the stoichiometric dissociation number, μ_s is the solute molality and ϕ_s is the molal or practical osmotic coefficient of the solute [3].

Since the molality is defined as the number of moles solute divided by the mass of the solvent [3], it could be calculated from the following relationship:

$$\mu_s = \frac{n_s}{\frac{\pi}{6}(D^3 - d_0^3)\rho_w} = \frac{\frac{m_s}{M_s}}{\frac{\pi}{6}(D^3 - d_0^3)\rho_w} \tag{18}$$

The molal osmotic coefficient of the solute was found from:

$$\phi_s = 1 - \mid z_1 z_2 \mid \left(A_\phi \frac{\sqrt{I}}{1 + b\sqrt{I}}\right) + \mu_s \frac{2v_1v_2}{v_s}\left(\beta_0\beta_1 e^{-\alpha\sqrt{I}}\right) + \mu_s^2 \frac{2(v_1v_2)^{\frac{3}{2}}}{v_s} C_\phi \tag{19}$$

where v_1 and v_2 are the numbers of positive and negative charges produced during dissociation, $\mid z_1 \mid$ and $\mid z_2 \mid$ are the number of elementary charge carriers carried by the ions, and A_ϕ, α , b, β_0, β_1 and C_ϕ are constants [3]. I gives the ionic strength of the solution and can be calculated from:

$$I = 0.5\mu_s(v_1 z_1^2 + v_2 z_2^2) \tag{20}$$

The values used to calculate the critical super saturations for sodium chloride, ammonium sulfate and sucrose are shown in table 4.

Parameter	Sodium chloride	Ammonium sulfate	Sucrose
M_s [kg/mol]	0.0584428	0.1321395	0.3423
M_w [kg/mol]	0.0180153	0.0180153	0.0180153
ρ_d [kg/m^3]	2165	1770	1589
ρ_w [kg/m^3]	997.1	997.1	997.1
σ_w [J/m^2]	0.07220175	0.07220175	0.07220175
T [K]	298.15	298.15	298.15
i	-	-	1
$\mid z_1 \mid$	1	1	-
$\mid z_2 \mid$	1	2	-
v_1	1	2	-
v_2	1	1	-
v_s	2	3	-
A_ϕ [(kg/mol)$^{1/2}$]	0.3915	0.3915	-
C_ϕ [kg^2/mol^2]	0.00119	-0.0012	-
β_0 [kg/mol]	0.1018	0.0409	-
β_1 [kg/mol]	0.2770	0.6585	-
α [(kg/mol)$^{1/2}$]	2	2	-
b [(kg/mol)$^{1/2}$]	1.2	1.2	-

Table 4: The valused used to calculate the critical super saturation for sodium chloride [3], ammonium sulfate [3] and sucrose [7] from Köhler theory, valied at a temperature of 298.15 K.

Appendix B

Linear calibrations were made between the critical flow rates (Q_{50_i}) and critical super saturations (SS_{c_i}) of the calibrated aerosols. The method used to create the calibration curves is most commonly used for chemical analysis [8], but is also valid for this study. The formula used can be viewed in equation 21 [8].

$$SS_{c_i} = \overline{SS_c} + \frac{b_1(Q_{50_i} - \overline{Q_{50}})}{K} \pm \frac{t_{1-\alpha/2,v}}{K} s_{Q_{50}} \left[\frac{(Q_{50_i} - \overline{Q_{50}})^2}{\sum (SS_{c_i} - \overline{SS_c})^2} + \left(\frac{1}{n} + \frac{1}{m} \right) K \right]^{1/2} \tag{21}$$

The first part of equation 21 determines the linear calibration while the second part defines the confidence interval. In this study, the following values were used:

$\overline{SS_c}$ = the average critical super saturation

$\overline{Q_{50}}$ = the average critical flow rate

$n = N$ = the number of observations used to construct the calibration curve

$m = 1$ = the number of responses for each observation

$v = n + m - 3$ = the number of degrees of freedom

$1 - \alpha = 95\%$ = the confidence level

The values for $t_{1-\alpha/2,v}$ were found from "Statistiskteori med tillämpningar" [9]

The values for b_1, $s^2_{Q_{50}}$, $s^2_{b_1}$ and K were calculated from equations 22, 23, 24 and 25, respectively.

$$b_1 = \frac{N(\sum SS_{c_i} Q_{50_i}) - (\sum SS_{c_i})(\sum Q_{50_i})}{N(\sum SS_{c_i}^2) - (\sum SS_{c_i})^2} \tag{22}$$

$$s^2_{Q_{50}} = \frac{\sum (Q_{50_i} - \overline{Q_{50}})^2 - b_1^2 \left[\sum (SS_{c_i} - \overline{SS_c})^2 \right]}{N - 2} \tag{23}$$

$$s^2_{b_1} = \frac{s^2_{Q_{50}}}{\sum (SS_{c_i} - \overline{SS_c})^2} \tag{24}$$

$$K = b_1^2 - (t_{1-\alpha/2,v})^2 s^2_{b_1} \tag{25}$$

Appendix C

Set diameter (nm)	Initial voltage (V)	Initial calibration (nm)	Final voltage (V)	Final calibration (nm)
20.0	32.6	17.0	51.7	21.5
21.0	36.9	18.0	58.5	23.0
22.0	41.5	19.0	65.5	24.0
23.0	46.3	20.5	72.8	26.0
24.0	51.3	21.5	80.4	27.0
25.0	56.4	23.0	88.3	28.0
26.0	61.8	24.0	96.5	30.0
27.0	67.3	25.0	105.0	31.0
28.0	73.0	26.0	113.7	32.0
29.0	78.9	27.0	122.8	34.0
30.0	84.9	28.0	132.1	35.0
31.0	91.2	29.0	141.7	36.0
32.0	97.6	30.0	151.5	38.0
33.0	104.2	31.0	161.6	39.0
34.0	111.0	32.0	172.0	40.0
35.0	117.9	33.0	182.7	41.5
36.0	125.1	34.0	193.6	43.0
37.0	132.3	35.0	204.8	44.0
38.0	139.8	36.5	216.2	45.5
39.0	147.4	37.5	227.9	47.0
40.0	155.2	38.5	239.8	48.0
41.0	163.1	39.5	252.0	49.0
42.0	171.2	40.5	264.4	51.0
43.0	179.5	41.5	277.1	52.0
44.0	187.9	43.0	290.0	53.0
45.0	196.5	44.0	303.2	54.5
50.0	241.6	49.0	372.4	61.0
55.0	290.5	54.0	447.4	67.5
60.0	342.9	59.0	527.7	74.0
65.0	398.6	64.0	613.1	80.5

Set diameter (nm)	Initial voltage (V)	Initial calibration (nm)	Final voltage (V)	Final calibration (nm)
70.0	457.4	69.0	703.4	87.0
75.0	519.3	74.0	798.4	93.5
80.0	584.1	79.0	897.7	100.0
85.0	651.6	84.0	1001.3	107.0
90.0	721.8	89.0	1108.8	113.0
95.0	794.4	94.0	1220.2	120.0
100.0	869.3	99.0	1335.2	126.5
105.0	946.5	104.0	1453.6	133.0
110.0	1025.9	109.0	1575.3	140.0
120.0	1190.5	119.0	1827.9	153.0
130.0	1362.6	129.0	2091.8	166.5
140.0	1541.3	139.0	2365.8	180.0
150.0	1726.0	149.0	2649.2	194.0
160.0	1916.2	159.0	2940.9	207.0

Table 5: Values for the initial and final diameter calibration of the DMA.